CREEP BEHAVIOR AND MICROSTRUCTURAL STABILITY OF P23/P91 DISSIMILAR WELDS DURING CREEP AT 550°C

Jan HOLEŠINSKÝ[a], Vlastimil VODÁREK[a], Lucie STŘÍLKOVÁ[b], Zdeněk KUBOŇ[b]

[a] *VSB - Technical University of Ostrava, Ostrava, Czech Republic, EU, jan.holesinsky@vsb.cz*
[b] *Materials and Metallurgical Research Ltd., Ostrava, Czech Republic, EU*

Abstract

The paper deals with the study on creep behavior and minor phase evolution in two types of heterogeneous weld joints of P23 and P91 steels during long-term creep exposure at 550 °C. The filler material in Weld A corresponded to P91 steel and the filler metal in Weld B was similar to the chemical composition of P23 steel. The creep rupture tests on the cross-weld test pieces of both welds revealed that most failures occurred in the partly decarburized zones of P23 steel or WM23. The carbon redistribution and the minor phase evolution across the sharp P23/P91 interface were calculated using Thermocalc and Dictra computer packages. The experimental study on minor phase evolution using both EDX and SAED in TEM was in a good agreement with the computer simulations, except for $M_{23}C_6$ phase in P23 (WM23) steel. EBSD technique used to study on microstructure changes along the P23/P91 boundary confirmed the slowing down of the recovery/recrystallization processes in the partly decarburized zone of HAZ of the P23 steel thanks to the presence of undissolved particles of M_6X and MX phases. Furthermore, the formation of Laves phase was proved in the partly decarburized zone of P23 steel. EBSD results also confirmed higher resistance of Weld A to softening processes in the partly decarburized zone of P23 steel compared to Weld B, which was in accordance with the results of creep rupture tests.

Keywords: Dissimilar welds, creep behavior, microstructural evolution, microstructural modeling

1. INTRODUCTION

The differences in temperature, pressure and corrosive/oxidation environment in different parts of boiler units in modern coal fired power plants with improved thermal efficiency are often compensated by heterogeneous weld joints of 2.5CrMo(W)V and advanced creep resistant (9-12)Cr steels [1; 2]. Dissimilar welds usually represent critical locations of power plant constructions and that is why a much of effort has to be devoted to studies on creep resistance and microstructural stability of these joints [3]. Redistribution of interstitial elements such as carbon and nitrogen strongly affects microstructural stability of dissimilar welds during thermal/creep exposure and it is driven by the differences in the activities of these elements across the fusion line [4]. These „up-hill“ diffusion processes lead to decarburization of low alloy steel adjacent to the fusion zone where the activities of interstitial elements are higher than on the side of high alloy steel. Such decarburization during exposure at elevated temperature can cause progressive weakening in this area and it represents a very important mechanism of microstructural degradation of dissimilar welds [1]. Progress in thermodynamic and kinetic microstructural modeling makes it possible to simulate microstructural evolution in heat resistant steels and their welds during long-term exposure [5]. However, experimental validation is needed. The creep characteristics in the individual weld regions and the way in which they interact as a consequence of the given load largely affect the deformation response of weldment. Discrepancy in the creep deformation rates exhibited by the parent, heat affected zone (HAZ) and weld metals can lead to the ductility exhaustion and accumulation of strain in the narrow zone leading to preferential crack nucleation sites and higher crack growth rates. Creep damage can simultaneously develop in several parts of cross-weld specimens and the final failure occurs in the weakest area for the given parameters of creep testing [6]. The paper is aimed at study on long - term creep rupture tests and microstructural stability of the P23/P91 dissimilar welds at 550 °C.

2. EXPERIMENTAL MATERIALS AND PROCEDURES

P23 and P91 steel pipes of the dimensions ϕ219 x 25 mm were welded in two ways. P91 matching filler metal (E CrMo 9 1B) was used in the Weld A and P23 matching consumable (Thyssen Cr2WV) in the Weld B. Detailed information about welding processes and post weld heat treatment (PWHT) is stated in [7]. The chemical compositions of base materials (BM) and weld metals (WM) are shown in **Table 1**.

Table 1 Chemical compositions of base metals and weld materials, wt. %

Material	C	Mn	Si	Cu	Ni	Cr	Mo	V	Ti	Nb	W	N	Al
P23	0.08	0.55	0.27	0.04	0.08	2.11	0.07	0.23	0.06	0.01	1.70	0.013	0.012
WM23	0.07	0.44	0.20	0.04	0.17	2.47	0.06	0.25	0.01	0.02	1.62	0.018	N.A.
P91	0.11	0.51	0.38	0.17	0.42	8.67	1.00	0.23	0.01	0.07	0.01	0.048	0.012
WM91	0.11	0.66	0.21	0.04	0.82	9.50	1.02	0.22	0.01	0.04	0.06	0.028	N.A.

Uniaxial creep tests were performed in air using cross-weld specimens (ϕ 6 mm), which included both BM and WM and also heat affected zones, at five stress levels in the range from 100 MPa to 150 MPa and at temperature of 550 °C. Failure locations of creep ruptured specimens were identified on the longitudinal sections by optical microscopy. EBSD technique in a scanning electron microscope Quanta 450 FEG was used to study recovery/recrystallization processes along the fusion line of P23/WM91 and P91/WM23, respectively. Study on the minor phase evolution during creep exposure at 550 °C was performed on carbon extraction replicas using both EDX technique and selected area diffraction (SAED) in a transmission electron microscope (TEM) JEOL JEM 2100. The replicas were prepared in the following regions of crept specimens: weld metal, base materials, decarburized and carburized zones of welds. Times to rupture of specimens used for detailed electron microscopy investigations were close to 30,000 hours, particularly 26,386 hours and 32,669 hours for the specimens A4 and B5, respectively. Thermodynamic equilibrium was calculated using Steel 16 database in Thermocalc software [8]. Dictra software and Steel 16 database were used for modeling of carbon redistribution and phase profiles across the P23/P91 interface without any fusion zone for 550 °C/30,000 hours [8].

3. RESULTS

3.1 Creep rupture behavior

Fig.1 shows the results of creep tests of Weld A and Weld B at 550 °C and the mean and low (-20% of the mean value) standardized creep rupture strength curves for P23 steel. The experimental values of creep rupture tests on cross-weld specimens of both designs of welds lie close to the -20% creep rupture strength curve for P23. Generally, the creep rupture results of Weld B were worse than that of Weld A. Metallographic investigations revealed that all specimens, except of the specimen A1, failed in the partly decarburized zones, **Fig.1**.

3.2 Microstructural modeling

Carbon redistribution across the sharp P23/P91 interface was calculated for 550 °C/30,000 hours, **Fig. 2a**. Up-hill diffusion of carbon from P23 up to 0.35 wt. % on the side of P91 was predicted. **Fig. 2b** shows the minor phase profiles across the sharp P23/P91 interface. The intensive dissolution of M_7C_3 phase due to carbon depletion in the partly decarburized zone of P23 is evident. The predicted decrease of MX and M_6X molar fractions in the vicinity of the P23/P91 interface is negligible. In the carburized zone of the P91 steel a high molar fraction of $M_{23}C_6$ and dissolution of Laves phase was predicted.

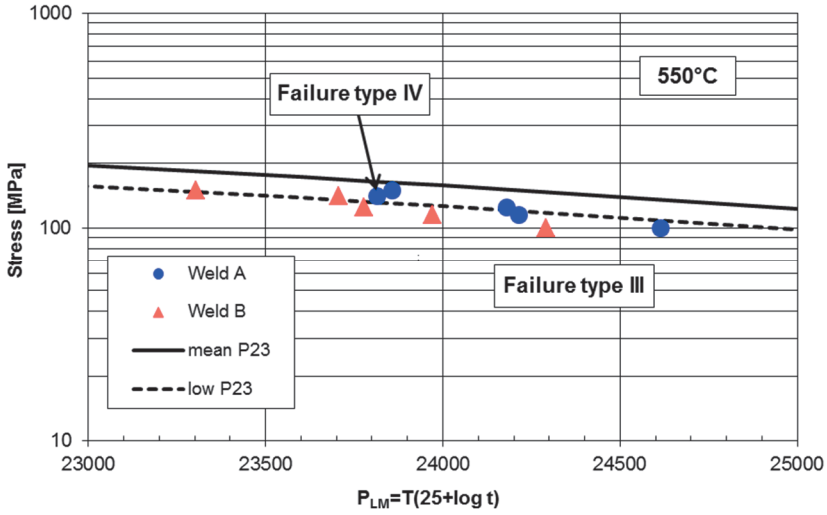

Fig. 1 Results of creep rupture tests of cross-weld specimens at 550 °C, all specimens, except of the specimen A1 (Failure type IV), failed in the partly decarburized zone (Failure type III)

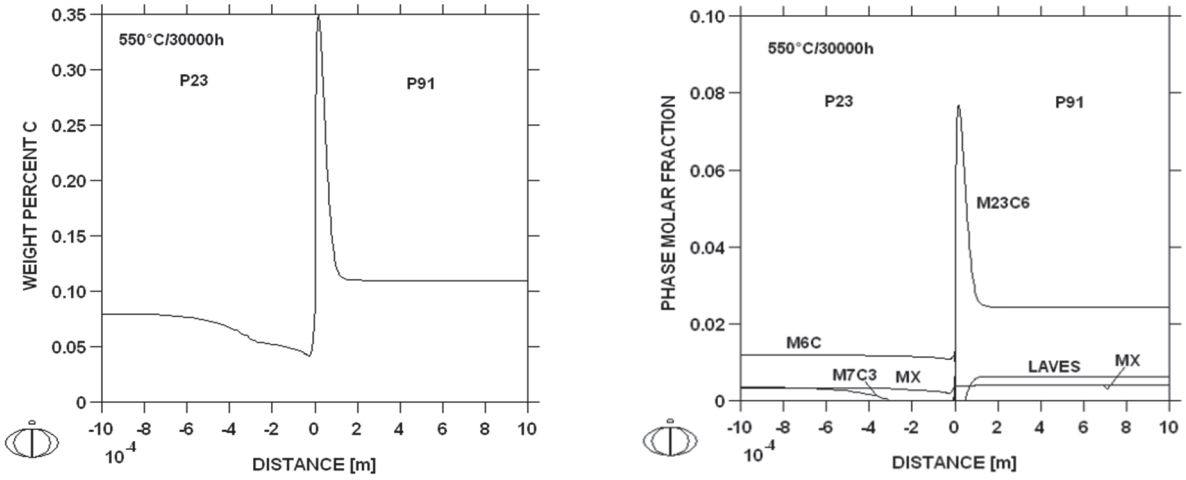

a) b)

Fig. 2 (a) Carbon redistribution and (b) phase profiles across the P23/P91 sharp interface for exposure of 550 °C/30,000 hours

3.3 Microstructural investigations

Combinations of inverse pole figure (IPF) and image quality (IQ) maps in the neighborhood of the WM91/P23 (specimen A4) and P91/WM23 (specimen B5) fusion line are shown in **Figs. 3a** and **3b**, respectively. It can be seen that the microstructure in the partly decarburized zone in the coarse grained part of heat affected zone (CGHAZ) of P23 in the specimen A4 remained bainitic up to the fusion boundary. However, recovery processes in bainite, which can be indicated by differences in color shading inside individual bainitic laths on the side of P23 (**Fig. 3a**), took place during creep exposure at 550 °C. The new recrystallized grains of ferrite were not obvious in the specimen A4. In the case of the specimen B5 small equiaxed recrystallized ferritic grains were observed in the vicinity of WM23/P91 fusion line in the partly decarburized layer of WM23 and the bainitic laths in this area were no more evident, **Fig. 3b**. The dark spots in the WM23 are complex oxides formed during welding in the weld metal. The recrystallization of bainite in WM23 in the specimen B5 was also proved by microhardness measurements.

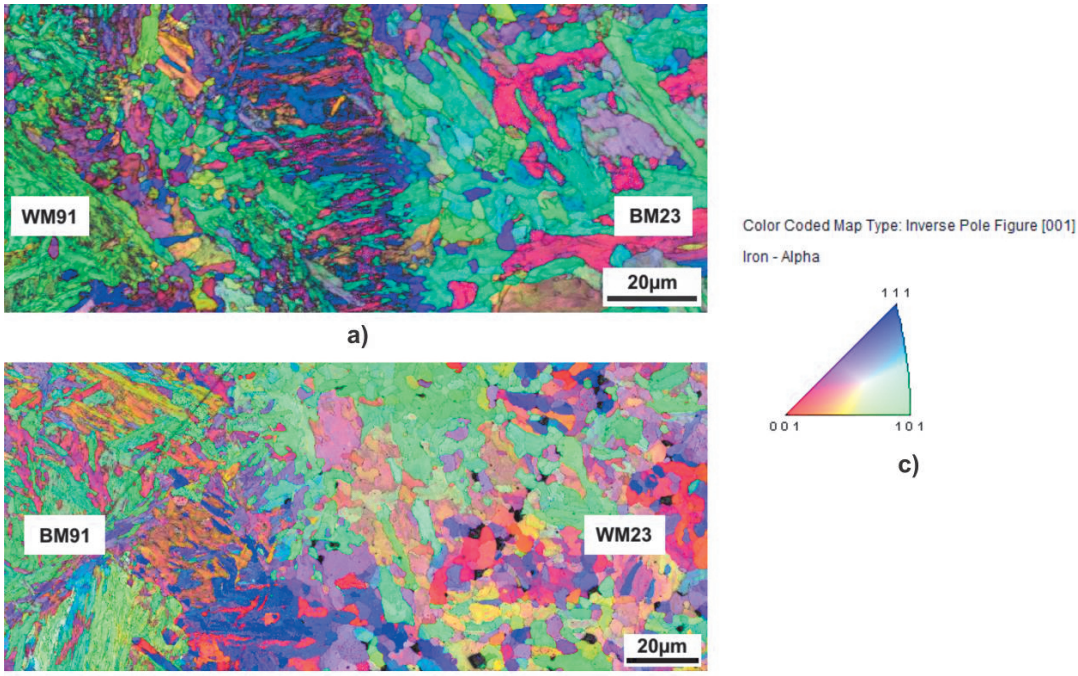

Fig. 3 Combination of IPF (ND) and IQ maps in the area of carbon redistribution across the fusion line: (a) P23/WM91 (specimen A4), (b) P91/WM23 (specimen B5), (c) legend with color coding

Results of experimental investigations on minor phases in the specimen A4 are summarized in **Table 2**. Minor phases identified in martensitic P91 steel are in accordance with the results of Thermocalc modeling. Coarse particles of Laves phase (Fe_2Mo) and particles of $M_{23}C_6$ of variable sizes decorated prior austenite grain boundaries and martensite lath boundaries, MX particles were mostly present inside martensitic laths, **Fig. 4a**. Z-phase particles were not found. Two types of MX particles were identified by EDX in BM91: coarse primary MX particles were rich in niobium (NbX) and fine secondary MX particles which contained vanadium and niobium.

Table 5 Minor phase identification, specimen A4

Area	Minor phases
BM P23	M_7C_3, $M_{23}C_6$, M_6X, MX
P23 decarb. zone	MX, M_6X, Laves phase
WM91 carb. zone	$M_{23}C_6$, MX, M_6X
BM P91	$M_{23}C_6$, NbX, secondary MX, Laves phase

Heavy precipitation in the carburized P23/WM91 fusion zone of the specimen A4 is shown in **Fig. 4**b. Precipitates of variable shapes and dimensions can be observed. SAED and EDX studies revealed that most precipitates were formed by $M_{23}C_6$ phase, insert in **Fig. 4b**. Some fine precipitates were identified as niobium rich MX particles. Chemical composition of $M_{23}C_6$ phase in the carburized band systematically changed from the side of P23 steel to WM91. Generally, more chromium in the matrix of the fusion zone less iron is in $M_{23}C_6$ particles. This was related to the chromium gradient in the carburized fusion zone. In the carburized layer on the side of P23 steel a small number density of M_6X particles coexisted with $M_{23}C_6$ particles. No Laves phase particles were found in the carburized band. Some differences between calculations and experimental findings were revealed in the case of the bainitic P23 base material. Particles of $M_{23}C_6$ phase were identified besides the predicted thermodynamically stable minor phases MX, M_7C_3 and M_6X. Calculations, carried out using the STEEL 16 database, consider $M_{23}C_6$ phase as a metastable phase in P23 steel. Precipitation in the P23 base material of the specimen A4 is shown in **Fig. 5a**. Coarse particles mainly consist of M_6X and $M_{23}C_6$ phases.

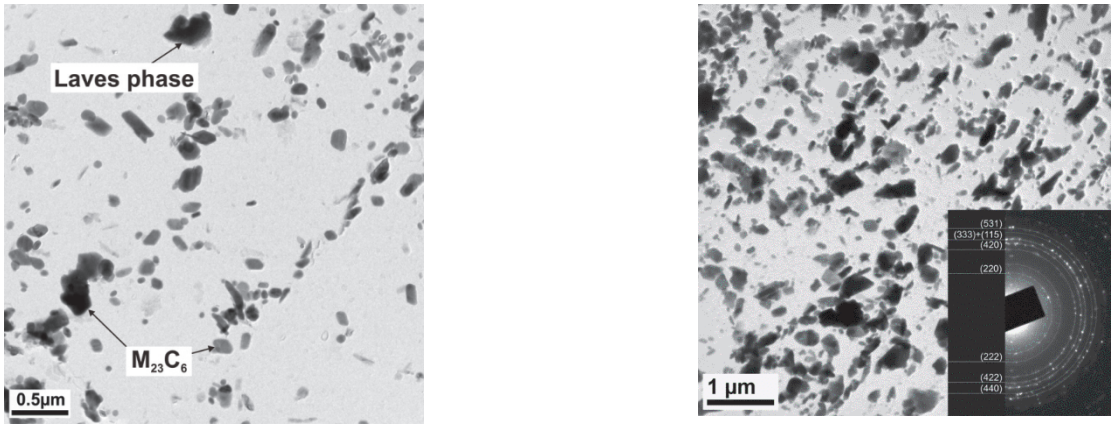

Fig. 4 Precipitation in specimen A4 (a) base material P91, (b) carburized zone of HAZ WM91, ring diffraction pattern of $M_{23}C_6$ phase

Experimental investigations on minor phase particles in the partly decarburized zone of CGHAZ of the P23 base material revealed that $M_{23}C_6$ as well as M_7C_3 particles completely dissolved during long-term creep exposure at 550 °C. However, rectangular TiX particles as well as fine MX particles rich in vanadium and tungsten were preserved in this area, Fig.5b. Furthermore, low density of particles with size about 200 nm rich in tungsten and iron was observed. SAED studies on these particles revealed two minor phases: M_6X and Fe_2W Laves phase. Due to planar defects on the basal plane (001) of Laves phase spot diffraction patterns revealed pronounced streaking, insert in **Fig. 5b**. The chemical compositions of both these phases in the partly decarburized zone of P23 are shown in **Table 3**. Precipitation of Laves phase in P23 steel was observed only in the partly decarburized layer, close to the fusion zone, on the contrary to M_6X particles.

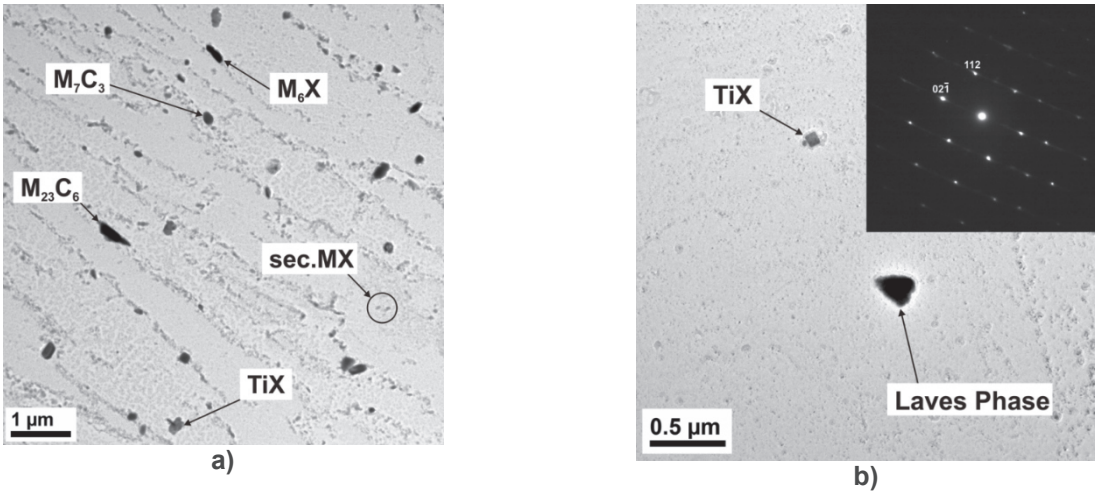

Fig. 5 Precipitation in specimen A4 (a) base material P91, (b) partially decarburized part of CGHAZ of BM23 spot diffraction pattern of Lves phase with zone axis$[\bar{5}12]_\eta$

Table 6 Chemical compositions of M_6X and Laves phase in the partly decarburized zone of P23 steel specimen A4, wt. %

Phase	V	Cr	Fe	Mo	W
M_6X	1.2	3.1	28.4	6.9	60.5
Laves phase	N.A.	2.9	32.9	5.7	58.5

CONCLUSIONS

Creep rupture tests on cross-weld specimens of dissimilar P23/P91 welds at 550 °C revealed higher creep resistance of Weld A with the filler material matching P91 steel compared to Weld B with the weld consumable corresponding to P23 steel. Creep failures of most specimens occurred in the partly decarburized area of P23 (WM23) steel close to the fusion line. This location of dissimilar welds is expected to be prone to creep damage due to redistribution of interstitial elements during both the PWHT and creep exposure.

Results of microstructural modelling of P23/P91 welds for 550 °C/30,000 hours were in a good agreement with experimental findings, except for $M_{23}C_6$ phase in P23 steel.

Based on EBSD investigations, Weld A was found to be more resistant to recovery/recrystallization processes in the partly decarburized zone than Weld B and it was in a good agreement with results of creep rupture tests.

Partial decarburization of P23 (WM23) steel in the course of creep exposure at 550 °C was accompanied by dissolution of M_7C_3 and $M_{23}C_6$ particles. Furthermore, decarburization of P23 steel resulted in precipitation of Laves phase (Fe_2W). In the carburized part of P91 (WM91) steel a high number density of $M_{23}C_6$ particles was identified. Changes in the composition of $M_{23}C_6$ particles proved that the carburized band was partly lying in the fusion zone.

ACKNOWLEDGEMENTS

The authors wish to acknowledge the financial support from the projects No. LO1203 "Regional Materials Science and Technology Centre - Feasibility Program" funded by Ministry of Education, Youth and Sports of the Czech Republic and SP2014/73.

REFERENCES

[1] ALLEN, D. J., Creep Performance of Dissimilar P91 to Low Alloy Steel Weldments, Proc. *Parsons 2003 - Engineering Issues in Turbine Machinery, Power Plant and Renewables*, Strang A. et al., Eds., IOM, London 2003, pp. 281-294.

[2] BARNARD, P.M., BUCHANAN, L.W., BARRIE M., Material Development for Supercritical Boiler Pipeworks, In: *Materials for Advanced Power Engineering 2010*, J. Lecomte - Beckers et.al. Eds., Forschungszentrum Jűlich, 2010, pp. 39 - 54.

[3] HEUSER, H., JOCHUM, C., BENDICK, W., HAHN, B., Welding of New Pipe Steels in Modern High Efficiency Power Stations with high Steam Parameters, In: *Safety and Reliability of Welded Components in Energy and Processing Industry*, Verlag TU Graz, Graz, 2008, pp. 67 - 74.

[4] KOZESCHNIK, E., *Dissimilar 2.25Cr/9Cr and 2Cr/0.5CrMoV Steel Welds*, Science and Technology of Welding and Joining, vol. 7, 2002, pp. 63 - 69.

[5] KOZESCHNIK, E. *Modelling Solid - State Precipitation*, Momentum Press, LLC, 2013, pp. 1 - 464

[6] VODÁREK V., KUBOŇ Z., FORET R., HAINSWOTH S., Microstructural Evolution in P23/P91 Heterogeneous Welds during Creep at 500 - 600°C, Proc. *Safety and Reliability of Welded Components in Energy and Processing Industry*, Verlag TU Graz, Graz, 2008, pp. 233-238.

[7] PECHA, J., Bošanský, J., *Welding of Similar and Dissimilar Steels*, COST 522 Progress Report, SES Tlmače-WRI, Bratislava, 2002, pp.28.

[8] ZLÁMAL, B., FORET, R., SOPOUŠEK J. *Modelling of Phase Compositions of P23 and P91 Steels and their Welds*, Technical Report, VUT Brno, 2007, pp. 1 - 28 (in Czech).